



1 **Significant production of ClNO₂ and possible source of Cl₂ from N₂O₅ uptake at a**
2 **suburban site in eastern China**

3 Men Xia^a, Xiang Peng^a, Weihao Wang^a, Chuan Yu^a, Peng Sun^b, Yuanyuan Li^b, Yuliang Liu^b,
4 Zhengning Xu^b, Zhe Wang^{a,c}, Zheng Xu^b, Wei Nie^b, Aijun Ding^b, and Tao Wang^{a,*}

5 ^aDepartment of Civil and Environmental Engineering, The Hong Kong Polytechnic University,
6 Hong Kong, China

7 ^b Joint International Research Laboratory of Atmospheric and Earth System Sciences, School
8 of Atmospheric Sciences, Nanjing University, Nanjing, 210023, China

9 ^c Now at Division of Environment and Sustainability, Hong Kong University of Science and
10 Technology, Hong Kong, China

11 * *Correspondence to:* Tao Wang (cetwang@polyu.edu.hk)

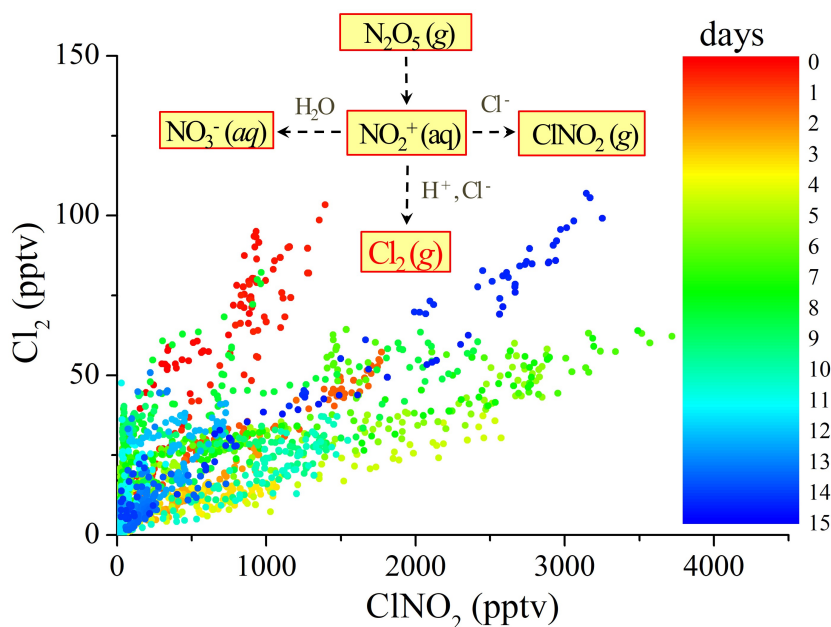
12

13 **Abstract**

14 ClNO₂ and Cl₂ can affect atmospheric oxidation and thereby the formation of ozone and
15 secondary aerosols, yet their sources and production mechanisms are not well understood or
16 quantified. In this study we present field observations of ClNO₂ and Cl₂ at a suburban site in
17 eastern China during April 2018. Persistent high levels of ClNO₂ (maximum ~3.7 ppbv; 1 min
18 average) were frequently observed at night, due to the high ClNO₂ yield ($\phi(\text{ClNO}_2)$, 0.56 ± 0.20)
19 inferred from the measurements. The $\phi(\text{ClNO}_2)$ value showed a positive correlation with the
20 $[\text{Cl}^-]/[\text{H}_2\text{O}]$ ratio, and its parameterization was improved by the incorporation of $[\text{Cl}^-]/[\text{H}_2\text{O}]$
21 and the suppression effect of aerosol organics. ClNO₂ and Cl₂ showed a significant correlation
22 on most nights. We show that the Cl₂ at our site was likely a co-product with ClNO₂ from N₂O₅
23 uptake on aerosols that contain acidic chloride, rather than being produced by ClNO₂ uptake,
24 as previously suggested. The Cl₂ yield ($\phi(\text{Cl}_2)$) derived from the N₂O₅ uptake hypothesis
25 exhibited significant correlations with $[\text{Cl}^-]$ and $[\text{H}^+]$, based on which a parameterization of
26 $\phi(\text{Cl}_2)$ was developed. The derived parameterizations of $\phi(\text{ClNO}_2)$ and $\phi(\text{Cl}_2)$ can be used in
27 models to quantify the nighttime production of ClNO₂ and Cl₂ and their impact on the next
28 day's photochemistry.



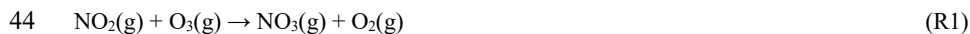
29 Graphical abstract

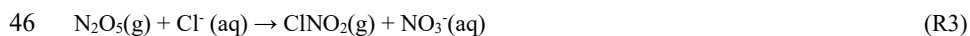


30

31 1. Introduction

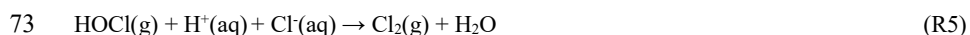
32 Chlorine radicals (Cl^\cdot) are potent oxidizers in the atmosphere (Seinfeld and Pandis, 2016).
33 Cl^\cdot destroy the O_3 layer in the stratosphere, exposing the biosphere to excess ultraviolet
34 radiation (Molina and Rowland, 1974). In the polluted troposphere, Cl^\cdot react with volatile
35 organic compounds (VOCs), especially alkanes, contribute to primary RO_x ($= \text{OH} + \text{HO}_2 + \text{RO}_2$)
36 production, and affect hydroxyl radical (OH) and O_3 concentrations (Simpson et al., 2015).
37 Nitryl chloride (ClNO_2) is a major chlorine radical precursor in the troposphere and has been
38 investigated around the globe over the past decade (Osthoff et al., 2008; Thornton et al., 2010;
39 Mielke et al., 2011; Wang et al., 2016). ClNO_2 is an important nocturnal reservoir of chlorine
40 and NO_x and is produced mostly at night. NO_x reacts with O_3 to form NO_3 radicals and N_2O_5
41 (Reactions R1 and R2). When aerosol chloride is present, ClNO_2 and nitrate are produced from
42 the heterogeneous uptake of N_2O_5 on aerosols (Reaction R3) (Finlayson-Pitts et al., 1989). After
43 sunrise, ClNO_2 is photolyzed to return NO_2 and release Cl^\cdot (Reaction R4).





48 Two key kinetic parameters for quantification of ClNO_2 formation are $\gamma(\text{N}_2\text{O}_5)$ (i.e., N_2O_5
49 uptake probability on aerosols) and $\phi(\text{ClNO}_2)$ (i.e., ClNO_2 production yield from N_2O_5 uptake)
50 (Thornton et al., 2003; Behnke et al., 1997). Laboratory studies have shown that $\phi(\text{ClNO}_2)$ is
51 dependent on the $[\text{Cl}^-]/[\text{H}_2\text{O}]$ ratio because aqueous Cl^- and H_2O compete for the NO_2^+
52 intermediate, based upon which a parameterization was developed to predict $\phi(\text{ClNO}_2)$
53 (hereafter denoted as $\phi(\text{ClNO}_2)_{\text{BT}}$) (Bertram and Thornton, 2009). The parameterization was
54 tested in several field studies, and it was found that the parameterized $\phi(\text{ClNO}_2)$ values were
55 significantly larger than the field-derived values (Tham et al., 2016; Wang et al., 2017; Tham
56 et al., 2018; McDuffie et al., 2018b; Staudt et al., 2019). The exact causes of these discrepancies
57 are not fully understood. The suppression of $\phi(\text{ClNO}_2)$ has been observed in biomass-burning
58 plumes in north China, but the specific species that reduced $\phi(\text{ClNO}_2)$ were not identified
59 (Tham et al., 2018). Some inorganic nucleophiles such as sulfate and organic nucleophiles such
60 as acetate were recently proposed to decrease $\phi(\text{ClNO}_2)$ by consuming NO_2^+ (McDuffie et al.,
61 2018b; Staudt et al., 2019). Such NO_2^+ -consuming nucleophiles may generate products from
62 N_2O_5 uptake other than ClNO_2 and nitrate, and this is deserving of further investigation.

63 Besides ClNO_2 , Cl_2 is another important chlorine radical precursor that is present in the lower
64 troposphere (Spicer et al., 1998; Custard et al., 2016; Priestley et al., 2018). Elevated levels of
65 Cl_2 (up to ~400 pptv) have been observed during the daytime in polar and continental
66 environments (Liao et al., 2014; Liu et al., 2017), whereas other studies found nocturnal peaks
67 of Cl_2 mixing ratios in polar, coastal, and continental sites (Mielke et al., 2011; Riedel et al.,
68 2012; Riedel et al., 2013; McNamara et al., 2019). Several potential sources of Cl_2 have been
69 proposed, such as direct emissions from power plants (Riedel et al., 2013) and water treatment
70 facilities (Mielke et al., 2011), photochemical formation associated with O_3 (Liao et al., 2014),
71 and heterogeneous conversion from chlorinated compounds (Reactions R5 and R6) (Deiber et
72 al., 2004; Pratte and Rossi, 2006; McNamara et al., 2019).





75 Cl_2 can also be produced from heterogeneous N_2O_5 uptake on acidic aerosols laden with
76 chloride, and $\text{ClNO}_2(\text{aq})$ has been proposed as an intermediate in Cl_2 production (Reaction R7)
77 on the basis of laboratory studies (Roberts et al., 2008; Roberts et al., 2009).



79 Significant correlations of ClNO_2 and Cl_2 were observed during an airborne campaign in the
80 United States and were interpreted as evidence of Cl_2 production from ClNO_2 uptake on acidic
81 aerosols (Haskins et al., 2019). However, this study also found that Cl_2 formation from ClNO_2
82 uptake was less efficient, because the estimated $\gamma(\text{ClNO}_2)$ value $((2.3 \pm 1.8) \times 10^{-5})$ was two
83 orders of magnitude lower than that suggested by laboratory studies $((6.0 \pm 2.0) \times 10^{-3})$ (Roberts
84 et al., 2008; Haskins et al., 2019). It remains unclear whether ClNO_2 uptake proceeds more
85 slowly in ambient environments than in laboratory conditions or whether additional pathways
86 are responsible for the formation of Cl_2 . Therefore, the detailed activation process by which
87 inert chlorine (e.g., particulate chloride) is converted to reactive chlorine remains highly
88 uncertain and requires further research.

89 In April 2018, we conducted field measurements of ClNO_2 , Cl_2 , and other trace gases and
90 aerosols in a suburban area of the Yangtze River Delta (YRD), a highly populated and
91 industrialized region in eastern China. High levels of ClNO_2 with enhanced Cl_2 were observed
92 at night. In this study, we investigated the activation of chlorine initiated by heterogeneous N_2O_5
93 chemistry. We first introduce prominent features of the observation results. The key parameters
94 in ClNO_2 formation (i.e., $\gamma(\text{N}_2\text{O}_5)$ and $\phi(\text{ClNO}_2)$) are then derived using the ambient data.
95 Factors that influence $\phi(\text{ClNO}_2)$ are discussed, with a focus on a revision of the
96 parameterization of $\phi(\text{ClNO}_2)$. We present observational evidence for a possible co-production
97 pathway of Cl_2 with ClNO_2 from heterogeneous reactions of N_2O_5 and propose a new
98 parameterization for nocturnal formation of Cl_2 .

99

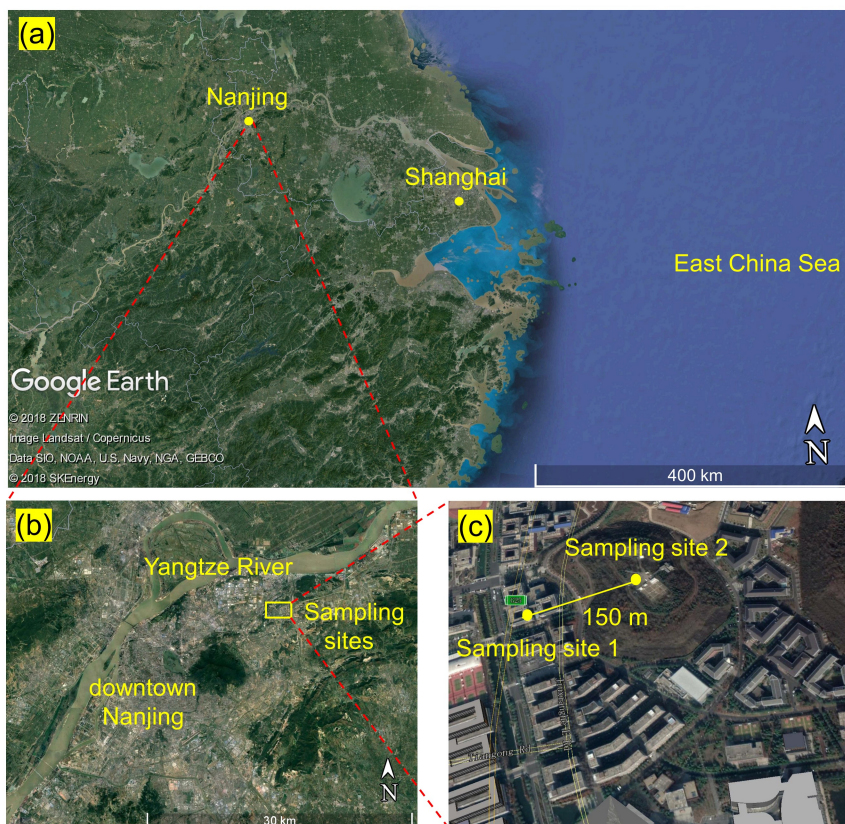
100 2. Methods

101 2.1 Observation sites



102 The field campaign was conducted from 11 to 26 April, 2018 on the Xianlin Campus of
103 Nanjing University, which is situated in a suburban area approximately 20 km northeast of
104 downtown Nanjing (see Fig. 1). The observation sites are surrounded by teaching and
105 residential buildings, sparse roads, and vegetation cover for about 1 to 2 km, with no significant
106 emission sources. Approximately 15 km northwest of the sampling sites are large-scale
107 chemical and steel facilities, which can be sources of gaseous pollutants (CO, SO₂, NO_x, and
108 VOCs) and particulate matters that may influence the site (Zhou et al., 2017). In addition,
109 Shanghai is approximately 270 km southeast of the measurement site.

110 The main data reported in this study (i.e., N₂O₅, ClNO₂, and Cl₂) and the NO_x and O₃ data
111 were obtained at the School of Atmospheric Sciences (SAS) of Nanjing University (sampling
112 site 1). The auxiliary data, including O₃, VOCs, aerosol size distribution, and chemical
113 composition, were obtained at the Station for Observing Regional Processes of the Earth
114 System (SORPES, sampling site 2). Fig. 1 shows the locations of the two sampling sites.
115 Interested readers are referred to previous studies for more information about the SORPES site
116 (e.g., Ding et al., 2013; Sun et al., 2018; Ding et al., 2019). A comparison of O₃ measurements
117 at the SAS and SORPES sites shows excellent agreement during the observation period (Fig.
118 S1).



119
120 **Figure 1.** Sampling locations. (a) Location of Nanjing city in the YRD region. (b) Location of
121 sampling sites in Nanjing. (c) Sampling sites 1 and 2 on the Xianlin campus of Nanjing
122 University. (© Google Earth)

123

124 2.2 N₂O₅, ClNO₂, and Cl₂ measurements

125 A chemical ionization mass spectrometer coupled with a quadrupole mass analyzer (Q-
126 CIMS, THS Instruments) was used to detect N₂O₅, ClNO₂, Cl₂, and HOCl. The Q-CIMS had
127 been used in previous field campaigns to measure N₂O₅ and ClNO₂ (Wang et al., 2016; Tham
128 et al., 2016). In this study, we also measured Cl₂ and HOCl and tuned the pressure of the drift
129 tube reactor accordingly. The principles and ion chemistry of Q-CIMS were described in detail
130 by Kercher et al. (2009). Briefly, iodide (I⁻) was adopted as the primary ion for strong affinity
131 with our target species. Charged iodide clusters, such as IN₂O₅⁻, ICINO₂⁻, ICl₂⁻, and IHOCI⁻, are



132 formed by the ion molecular reactions shown in Reactions (R8) through (R11). Ion clusters with
133 different Cl isotopes (i.e., ^{35}Cl and ^{37}Cl) were recorded to examine the identity of ClNO_2 and
134 Cl_2 , and this isotopic analysis confirmed that ClNO_2 and Cl_2 had very minor interferences (see
135 Text S1).



140 The Q-CIMS was housed on the fifth floor of the SAS building. The PFA sampling tube
141 (length, 1.5 m; outer diameter, 0.25 in) extended out through a hole in the side wall. We took
142 precautions to minimize the deposition of particles on the inner wall of the sampling tube and
143 tested the possible formation and loss of N_2O_5 , ClNO_2 , and Cl_2 on the sampling tube (see Text
144 S1 for details), which showed a negligible inlet interference on the CIMS measurement. N_2O_5
145 and ClNO_2 were calibrated every two days following established methods (Wang et al., 2016).
146 Briefly, N_2O_5 was synthesized from the reaction of NO_2 and O_3 , and ClNO_2 was produced by
147 passing N_2O_5 through a deliquesced NaCl slurry. The dependence of N_2O_5 sensitivity on relative
148 humidity (RH) was tested on site (see Fig. S3) and was used to account for changes in ambient
149 RH. A Cl_2 permeation tube was used for Cl_2 calibration (Liao et al., 2014), and the permeation
150 rate of Cl_2 was quantified by chemical titration and ultraviolet spectrophotometry. We assumed
151 the sensitivity of HOCl to be the same as that of ClO , and we used a sensitivity ratio of ClO to
152 Cl_2 (0.26) that was experimentally determined by Custard et al. (2016). In this study, the HOCl
153 data were only used qualitatively. In sum, the sensitivities of N_2O_5 , ClNO_2 , Cl_2 , and HOCl were
154 0.42 ± 0.11 , 0.35 ± 0.13 , 0.86 ± 0.37 , and 0.22 ± 0.08 Hz/ppTV, respectively. The uncertainties
155 of the N_2O_5 and ClNO_2 measurements were estimated to be 19% via error propagation. The Cl_2
156 measurement uncertainty was estimated to be 15%. The details of CIMS calibrations and
157 uncertainty analysis are available in Text S1 and Table S3.

158

159 2.3 Auxiliary measurements



160 In addition to the CIMS measurement at the SAS site, meteorological factors, gaseous and
161 aerosol chemical compositions, particle size distributions, and the NO₂ photolysis frequency
162 (*j*NO₂) were simultaneously measured at the SORPES site (Table S1). The ionic compositions
163 of PM_{2.5}, including Cl⁻, NO₃⁻, SO₄²⁻, and NH₄⁺, were measured with an Aerosol Chemical
164 Speciation Monitor (ACSM, Aerodyne Research Inc.) and MARGA (Metrohm, Switzerland).
165 The hourly-averaged ionic compositions from ACSM and MARGA showed good agreement
166 (see Fig. S4). In addition, HNO₃ was also measured by MARGA. In this study, the 10-min
167 averaged ACSM data, including total organics, were used for subsequent analysis. The mass
168 concentration of H⁺ (μg/m³) was estimated to achieve electric charge balance of the cation
169 (NH₄⁺) and anions (Cl⁻, NO₃⁻, and SO₄²⁻) of the ACSM data. The molar concentrations of
170 inorganic ions (i.e., [Cl⁻], [NO₃⁻], [SO₄²⁻], [NH₄⁺], and [H⁺]) and total organics ([Org]) were
171 estimated using the extended aerosol inorganics model (E-AIM, model III) (Wexler, 2002). The
172 molecular weight of the organic molecules was assumed to be 250 g/mol (McDuffie et al.,
173 2018b). The dry-state submicron particle size distribution was measured with a Scanning
174 Mobility Particle Sizer (SMPS, TSI Inc.), and the data were used to estimate the aerosol surface
175 area density (S_a) with the assumption of spherical particles. The hygroscopic growth factor of
176 the particle size was based on an empirical parameterization, $GF = 0.582 \left(8.46 + \frac{1}{1 - RH} \right)^{1/3}$
177 (Lewis, 2008). The VOCs were measured with a proton transfer reaction time-of-flight mass
178 spectrometer (PTR-TOF-MS, Ionicon).

179

180 2.4 Production and loss of NO₃ and N₂O₅

181 NO₃ radicals are primarily produced from NO₂ and O₃ (Reaction R1). The production rate
182 equation of NO₃ (P(NO₃)) is shown as follows (Eq. (1)):

$$183 \quad P(\text{NO}_3) = k_1[\text{NO}_2][\text{O}_3] \quad (1)$$

184 where *k*₁ is the rate constant of Reaction R1. NO₃ is mainly removed by gas-phase reactions
185 with VOCs and NO (Eq. (2)) and heterogeneous loss via N₂O₅ uptake (Eq. (3)), where *k*(NO₃)
186 and *k*(N₂O₅) are the first-order loss rate coefficients of NO₃ and N₂O₅, respectively.

$$187 \quad k(\text{NO}_3) = k_{\text{NO} + \text{NO}_3}[\text{NO}] + \sum k_i[\text{VOC}_i] \quad (2)$$



$$k(\text{N}_2\text{O}_5) = \frac{1}{4}c(\text{N}_2\text{O}_5)S_a\gamma(\text{N}_2\text{O}_5) \quad (3)$$

where $k_{\text{NO}+\text{NO}_3}$ and k_i denote the reaction rate constants of NO_3 with NO and VOC , respectively, and $c(\text{N}_2\text{O}_5)$ is the average velocity of N_2O_5 molecules. Other minor loss pathways of NO_3 and N_2O_5 were not considered (e.g., homogeneous loss of N_2O_5).

192

193 2.5 Estimation of $\phi(\text{ClNO}_2)$ and $\gamma(\text{N}_2\text{O}_5)$

194 $\phi(\text{ClNO}_2)$ and $\gamma(\text{N}_2\text{O}_5)$ were estimated using the observation data and parameterization. We
195 used the observed increasing rates of ClNO_2 and total nitrate (i.e., $\text{HNO}_3+\text{NO}_3^-$) to derive the
196 values for $\gamma(\text{N}_2\text{O}_5)$ and $\phi(\text{ClNO}_2)$ in the selected cases (Phillips et al., 2016). Details of the
197 method are described elsewhere (Tham et al., 2016; Phillips et al., 2016). Briefly, the production
198 rate of ClNO_2 ($P(\text{ClNO}_2)$) is calculated as follows (Eq. (4)).

$$P(\text{ClNO}_2) = \frac{1}{4}c(\text{N}_2\text{O}_5)S_a\gamma(\text{N}_2\text{O}_5)[\text{N}_2\text{O}_5]\phi(\text{ClNO}_2) \quad (4)$$

199 The production rate of total nitrate induced by N_2O_5 uptake during the night ($P(\text{NO}_3^-)$) is shown
200 by Eq. (5).

$$P(\text{NO}_3^-) = \frac{1}{4}c(\text{N}_2\text{O}_5)S_a\gamma(\text{N}_2\text{O}_5)[\text{N}_2\text{O}_5](2-\phi(\text{ClNO}_2)) \quad (5)$$

203 $\phi(\text{ClNO}_2)$ is obtained by combining Eqs. (4) and (5).

$$\phi(\text{ClNO}_2) = 2\left(1 + \frac{P(\text{NO}_3^-)}{P(\text{ClNO}_2)}\right)^{-1} \quad (6)$$

205 And $\gamma(\text{N}_2\text{O}_5)$ is derived as follows (Eq. (7)).

$$\gamma(\text{N}_2\text{O}_5) = \frac{2(P(\text{ClNO}_2) + P(\text{NO}_3^-))}{c(\text{N}_2\text{O}_5)S_a[\text{N}_2\text{O}_5]} \quad (7)$$

207 This method assumes that: (1) air masses are relatively stable; and (2) N_2O_5 uptake dominates
208 NO_3^- production at night (Tham et al., 2018). Assumption (1) requires careful selection of the
209 cases of interest. Regarding assumption (2), major nocturnal production pathways of total
210 nitrate should be evaluated, such as comparing the reaction rate of N_2O_5 heterogeneous loss
211 ($k(\text{N}_2\text{O}_5)*[\text{N}_2\text{O}_5]$) with that of $\text{NO}_3 + \text{VOC}$ ($k(\text{NO}_3)*[\text{NO}_3]$), which may produce HNO_3 via H-
212 abstraction reactions.

213 $\phi(\text{ClNO}_2)$ was also calculated with the parameterization shown in Eq. (8), in which the k_4/k_3
214 ratio was adopted as 483 ± 175 (Bertram and Thornton, 2009).



$$\varphi(\text{ClNO}_2)_{\text{BT}} = \left(1 + \frac{[\text{H}_2\text{O}]}{k_4/k_3[\text{Cl}^-]}\right)^{-1} \quad (8)$$

216 When considering the potential competitive effect of other species (denoted as “Y⁻”), such as
217 sulfate or aerosol organics, for the NO₂⁺ intermediate, the following equation (Eq. (9)) was
218 established (McDuffie et al., 2018b). Rearrangement of Eq. (9) yields Eq. (10), in which
219 plotting $\left(\frac{1}{\varphi(\text{ClNO}_2)} - 1\right) * \frac{[\text{Cl}^-]}{[\text{H}_2\text{O}]}$ to $\frac{[\text{Y}^-]}{[\text{Cl}^-]}$ should exhibit a positive correlation. k_5 represents a
220 constant reaction rate coefficient of “Y⁻” with NO₂⁺.

$$\varphi(\text{ClNO}_2) = \frac{1}{1 + \frac{k_3[\text{H}_2\text{O}]}{k_4[\text{Cl}^-]} + \frac{k_5[\text{Y}^-]}{k_4[\text{Cl}^-]}} \quad (9)$$

$$\left(\frac{1}{\varphi(\text{ClNO}_2)} - 1\right) * \frac{[\text{Cl}^-]}{[\text{H}_2\text{O}]} = \frac{k_3}{k_4} + \frac{k_5[\text{Y}^-]}{k_4[\text{Cl}^-]} \quad (10)$$

223

224 3. Results and Discussions

225 3.1 Overall observation results

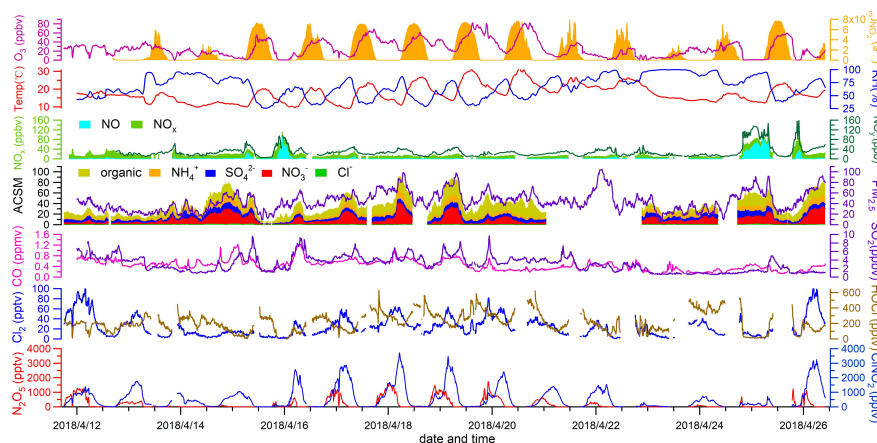
226 Fig. 2 depicts the time series of N₂O₅, ClNO₂, Cl₂, and related species. Overall, the
227 observation sites experienced moderate levels of pollution during the study period (PM_{2.5}, 44.8
228 ± 18.3 µg/m³; CO, 0.4 ± 0.2 ppmv; SO₂, 3.1±1.8 ppbv; NO_x, 18.1 ± 16.6 ppbv; O₃, 25.8 ± 18.4
229 ppbv). The on-site observations indicated mostly stagnant weather with low wind speeds (1 m/s
230 in average). No precipitation was observed except for the evening of 13 April from 22:00 to
231 22:30 local time. The nocturnal NO mixing ratios were usually near the detection limit of the
232 NO instrument, and the presence of abundant NO₂ and O₃ favored N₂O₅ formation and
233 subsequent heterogeneous processes.

234 The most salient features of the observation were the high levels of ClNO₂ and moderate
235 levels of Cl₂ that were present during the night. The ClNO₂ mixing ratios exceeded 1 ppbv on
236 12 of the 15 nights. The observed ClNO₂ levels were among the highest in the world, with a
237 peak mixing ratio (1-min average, 3.7 ppbv) slightly higher than that of north China (1-min
238 average, 2.1 ppbv) (Tham et al., 2016) but lower than that reported in south China (1 min
239 average, 8.3 ppbv) (Yun et al., 2018). The frequent occurrence of high ClNO₂ levels was favored
240 by several factors, including elevated levels of N₂O₅ (1 ppbv), humid weather (RH, 67.7 ±



241 20.7%), and chloride availability ($0.36 \pm 0.31 \mu\text{g}/\text{m}^3$) during the field campaign. When high
242 levels of ClNO_2 were observed, elevated concentrations of particulate nitrate as high as 40.8
243 $\mu\text{g}/\text{m}^3$ (10-min average) were also present. We noticed that ClNO_2 and particulate nitrate
244 concentrations both increased more rapidly after midnight than before midnight from 15 to 19
245 April, which is discussed further below.

246 Moderate levels of Cl_2 (up to 100 pptv) were also observed during the night. Cl_2 mixing ratios
247 exhibited a clear diurnal pattern, peaking at night and decreasing during the day due to
248 photolysis. The nocturnal peaks of Cl_2 mixing ratios showed discrepancies from some previous
249 observations in which an elevated levels of Cl_2 was found during the day (Liao et al., 2014; Liu
250 et al., 2017). The Cl_2 and ClNO_2 mixing ratios reached peaks synchronously during most nights,
251 and both species decreased in abundance or were absent in NO -rich plumes (e.g., the nights of
252 13 and 25 April), which suggests that Cl_2 and ClNO_2 were produced from common sources.
253 Similar nighttime correlations of Cl_2 and ClNO_2 were also observed in the United States and in
254 northern China (Qiu et al., 2019; Haskins et al., 2019). A subsequent analysis of the present
255 study aims to elucidate the nighttime formation processes of ClNO_2 and Cl_2 .



256
257 **Figure 2.** Time series of ClNO_2 , Cl_2 , and related measurements during field observations from
258 11 to 26 April 2018. Data gaps were caused by technical problems or calibrations.

259

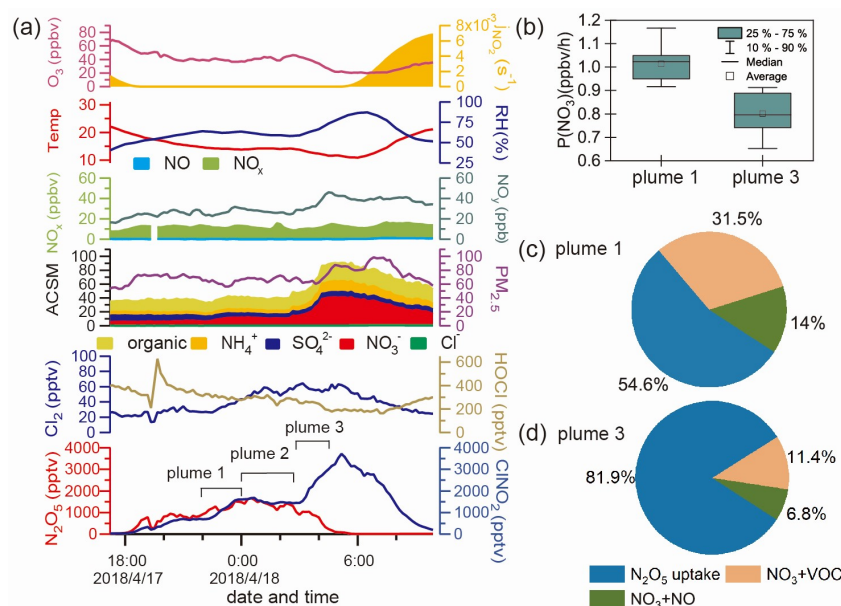
260 3.2 High ClNO_2 cases

261 Fig. 3 shows the observation results from 17 and 18 April to further illustrate the ClNO_2



262 formation process. This case had the highest ClNO₂ observed during the campaign and shows
 263 an example of high ClNO₂ mixing ratios after midnight. As shown in Fig. 3a, the mixing ratio
 264 of ClNO₂ began to increase after sunset (18:00 17 April) and decreased after midnight. The
 265 period between 22:00 and 24:00 on 17 April was noted as plume 1. After midnight, the ClNO₂
 266 mixing ratios exhibited a more rapid increase from 03:00 to 05:00 on 18 April (plume 3), and
 267 the particulate nitrate concentration also synchronously and significantly increased. Plumes 1
 268 and 3 were identified as being different, resulting from an air mass shift between 00:00 and
 269 03:00 on 18 April (plume 2), as indicated by abrupt changes in the RH, temperature, and O₃.
 270 We compared the backward trajectories from plume 1 to plume 3 and found no significant
 271 difference (figures not shown here). Thus, the change in the air mass from plume 1 to plume 3
 272 was likely a local phenomenon.

273 The P(NO₃) and NO₃ loss pathways during plumes 1 and 3 were calculated and compared in
 274 Fig. 3b-d using the methods described in Section 2.4. The P(NO₃) was slightly lower during
 275 plume 3 than during plume 1, and a larger proportion of NO₃ was lost via the N₂O₅ hydrolysis
 276 pathway in plume 3. Thus, the air mass shift, in addition to the higher rate of N₂O₅ hydrolysis,
 277 was responsible for the elevated ClNO₂ levels observed after midnight.



278



279 **Figure 3.** Detailed analysis of a high ClNO₂ episode observed on 17–18 April. **(a)** Time series
280 of ClNO₂ and related species. **(b)**, **(c)**, and **(d)** Comparisons of P(NO₃) and NO₃ loss pathways
281 in plumes 1 and 3.

282

283 3.3 ClNO₂ production yield from N₂O₅ uptake

284 $\phi(\text{ClNO}_2)$ was estimated to investigate its influencing factors and the performance of
285 parameterization in selected cases. The methods described in Section 2.5 were used to estimate
286 the $\phi(\text{ClNO}_2)$ and $\gamma(\text{N}_2\text{O}_5)$ using the observation data. As these methods assume a stable air
287 mass and the dominance of N₂O₅ uptake in nitrate formation, we applied the following criteria
288 when selecting cases for this analysis. First, the NO mixing ratios must be less than 0.1 ppbv.
289 When significant levels of NO were present, the N₂O₅ chemistry was suppressed. Second,
290 primary pollutants such as CO, SO₂, and meteorological factors (wind, temperature, and RH)
291 were required to exhibit relatively constant levels or stable trends within the cases. Third, the
292 ClNO₂ and nitrate levels had to be correlated ($R^2 > 0.6$) and show increasing trends. Fifteen
293 cases that lasted 30 min to 3 hours were selected, and 10-min averaged data were used for
294 calculation. Fig. S5 shows an example of this calculation, which corresponds to plume 1 on 17
295 April (Fig. 3). We then evaluated the loss pathways of NO₃ in the fifteen cases. The results show
296 that the NO₃ + VOCs reactions contributed less than one third of the total NO₃ + N₂O₅ loss (e.g.,
297 Fig. 3c, d). Nocturnal total nitrate production was thus dominated by N₂O₅ uptake, and only a
298 small proportion of nitrate was produced by NO₃+VOCs reactions.

299 The derived $\gamma(\text{N}_2\text{O}_5)$ values ranged from 0.004 to 0.014 (mean, 0.008 ± 0.004). The highest
300 $\gamma(\text{N}_2\text{O}_5)$ values (0.0135 and 0.0139) were derived between 03:00 and 05:00 on 18 April (i.e.,
301 plume 3 in Fig. 3), which was consistent with the rapid increase in ClNO₂ mixing ratios during
302 that period. The variations in the $\gamma(\text{N}_2\text{O}_5)$ value depended mainly on [H₂O] ($R^2 = 0.49$) (see Fig.
303 S6) but showed little correlation with other influencing factors, such as [Cl⁻], [NO₃⁻], and V_a/S_a
304 (figures not shown here). The dominant influence of [H₂O] on the $\gamma(\text{N}_2\text{O}_5)$ value was also
305 reported in a previous study in north China (Tham et al., 2018).

306 The $\phi(\text{ClNO}_2)$ value ranged from 0.28 to 0.89 (mean, 0.56 ± 0.15), which was among the



307 highest values in the world (McDuffie et al., 2018b). The $\varphi(\text{ClNO}_2)$ value in this study exhibited
308 an obvious nonlinear relationship with the $[\text{Cl}^-]/[\text{H}_2\text{O}]$ ratio ($R^2 = 0.52$) (Fig. 4a), which is
309 consistent with previous laboratory results (Bertram and Thornton, 2009). However, current
310 parameterization of $\varphi(\text{ClNO}_2)$ based on $[\text{Cl}^-]/[\text{H}_2\text{O}]$ ($\varphi(\text{ClNO}_2)_{\text{BT}}$) tended to overestimate the
311 observed $\varphi(\text{ClNO}_2)$ value (Fig. 4b).

312 Here we give two explanations for the inconsistency between the $\varphi(\text{ClNO}_2)_{\text{BT}}$ and the field-
313 derived $\varphi(\text{ClNO}_2)$. First, the reactivity of chloride with NO_2^+ (i.e., k_4/k_3 in Eq. 8) was reduced
314 in ambient environments due to complicated issues of the mixing state, phase state, and activity
315 coefficient. As $\varphi(\text{ClNO}_2)$ is positively dependent upon $[\text{Cl}^-]$, a reduction in chloride reactivity
316 could decrease the $\varphi(\text{ClNO}_2)$ value in ambient particles. This explanation is supported by
317 previous studies of $\gamma(\text{N}_2\text{O}_5)$ (Morgan et al., 2015; McDuffie et al., 2018a), which showed that
318 when the enhancement effect of chloride on $\gamma(\text{N}_2\text{O}_5)$ was neglected, the parameterized $\gamma(\text{N}_2\text{O}_5)$
319 better matched the observed $\gamma(\text{N}_2\text{O}_5)$. The second explanation deals with other unknown factors
320 that reduce the $\varphi(\text{ClNO}_2)$ value. The parameterization $\varphi(\text{ClNO}_2)_{\text{BT}}$ only considered the
321 $[\text{Cl}^-]/[\text{H}_2\text{O}]$ ratio, not other aqueous species that could suppress $\varphi(\text{ClNO}_2)$, leading to the
322 overestimation of $\varphi(\text{ClNO}_2)_{\text{BT}}$ values.

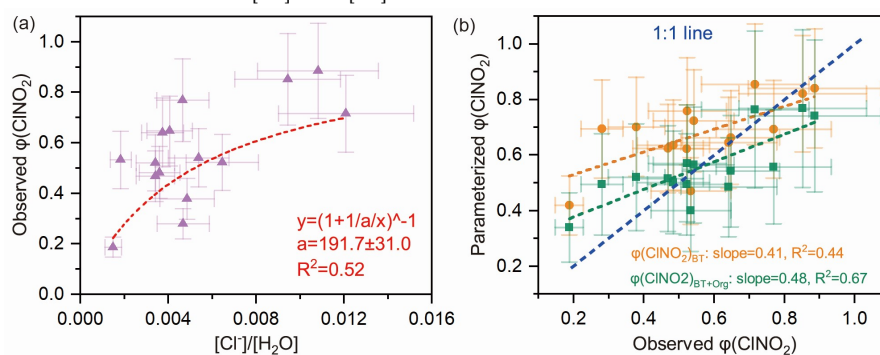
323 Regarding the second explanation, we examined the possibility of sulfate and aerosol
324 organics competing with $[\text{Cl}^-]$ for the NO_2^+ intermediate (see Section 2.4 and Eq. (10)). The
325 statistical results show that aerosol organics could reduce $\varphi(\text{ClNO}_2)$ values ($R^2 = 0.41$; Fig. S7b),
326 but sulfate did not show such an influence ($R^2 = 0.08$; Fig. S7a). The latter result contrasts with
327 the finding of a recent laboratory study, which indicated that both sulfate and some organics
328 (e.g., carboxylate) suppress ClNO_2 formation (Staudt et al., 2019).

329 By incorporating the suppression effect of aerosol organics, we performed regressions of
330 $\varphi(\text{ClNO}_2)$ and obtained an improved parameterization of $\varphi(\text{ClNO}_2)$ (noted as $\varphi(\text{ClNO}_2)_{\text{BT+Org}}$)
331 that better matched the observed $\varphi(\text{ClNO}_2)$ (Fig. 4b). In Eq. (11), the factor 483 (k_4/k_3 in Eq. 9)
332 was adopted from (Bertram and Thornton, 2009), and the factor 235 (k_4/k_5 in Eq. 9) was derived
333 here by iterative algorithms to achieve the least-square errors between the observed and
334 parameterized $\varphi(\text{ClNO}_2)$ values. Given that $k_4/k_3 = 483$ and $k_4/k_5 = 235$, k_5/k_3 was calculated as



335 2.06, which suggests that the reaction rate constant of aerosol organics with NO_2^+ was twice
336 that of the $\text{H}_2\text{O} + \text{NO}_2^+$ reaction. A recent laboratory study (Staudt et al., 2019) derived $k_5/k_3 =$
337 3.7 for acetate, which is very similar to our results.

$$338 \quad \varphi(\text{ClNO}_2)_{\text{BT+Org}} = \left(1 + \frac{[\text{H}_2\text{O}]}{483[\text{Cl}^-]} + \frac{[\text{Org}]}{235[\text{Cl}^-]}\right)^{-1} \quad (11)$$



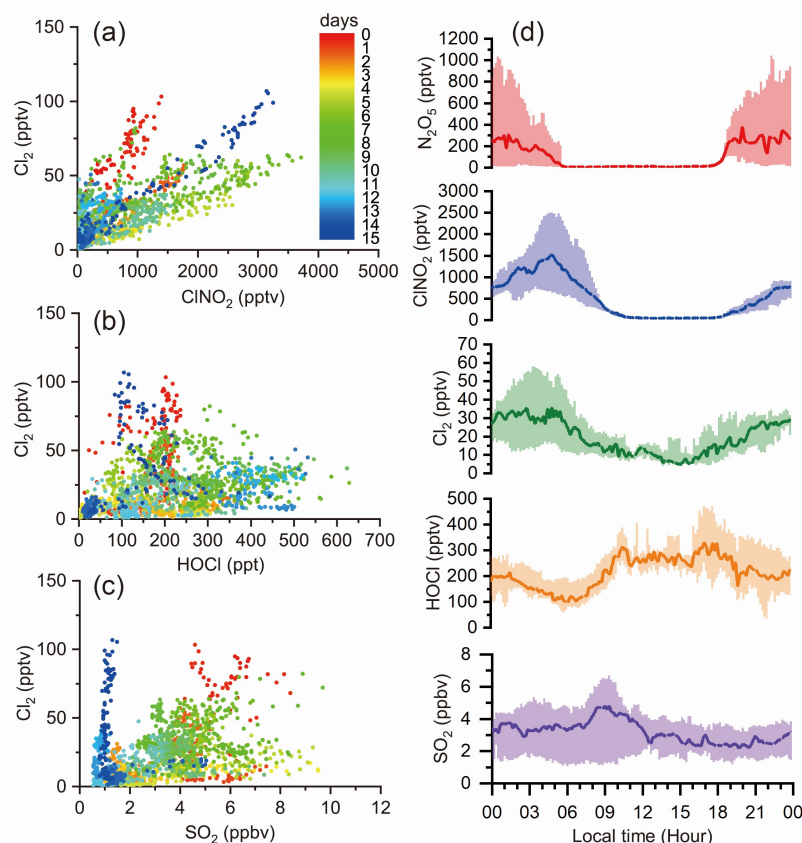
339
340 **Figure 4.** Influencing factors and parameterizations of $\varphi(\text{ClNO}_2)$. **(a)** Dependence of $\varphi(\text{ClNO}_2)$
341 on the $[\text{Cl}^-]/[\text{H}_2\text{O}]$ ratio. Dashed red line shows nonlinear fitting of $\varphi(\text{ClNO}_2)$; “a” represents
342 the k_4/k_3 in Eq. (8). **(b)** Comparison of parameterized $\varphi(\text{ClNO}_2)$ and observed $\varphi(\text{ClNO}_2)$, where
343 $\varphi(\text{ClNO}_2)_{\text{BT}}$ denotes the parameterization proposed by Bertram and Thornton (2009), and
344 $\varphi(\text{ClNO}_2)_{\text{BT+Org}}$ represents the revised parameterization used in this study (see Eq. (11)).

345

346 3.4 Nocturnal Cl_2 formation

347 3.4.1 Cl_2 as a co-product of ClNO_2 from N_2O_5 uptake

348 To elucidate the formation pathways of the elevated levels of Cl_2 observed during the night,
349 we investigated the correlations of Cl_2 with the ClNO_2 , HOCl , and SO_2 and the diurnal
350 variations of these (Fig. 5a–5d). Cl_2 only exhibited a significant correlation with ClNO_2 (Fig
351 5a). The $\text{Cl}_2/\text{ClNO}_2$ ratios varied on different nights, which implies that differences exist in the
352 production efficiencies of Cl_2 relative to those of ClNO_2 .



353

354 **Figure 5.** Correlations among Cl_2 , ClNO_2 , HOCl , and SO_2 and their diurnal profiles **(a)**, **(b)**,
355 and **(c)** show the correlations of Cl_2 with ClNO_2 , HOCl , and SO_2 respectively, during the whole
356 campaign. Dots represent 10-min averaged values colored according to campaign days. **(d)**
357 exhibits the diurnal variation of Cl_2 , ClNO_2 , HOCl , and SO_2 .

358

359 The current mainstream interpretation of the observed correlation of ClNO_2 and Cl_2 is that
360 Cl_2 is produced from ClNO_2 uptake (Ammann et al., 2013; Qiu et al., 2019; Wang et al., 2019;
361 Haskins et al., 2019). We provide evidence that this interpretation does not apply to
362 measurements from our site. We assessed the ClNO_2 uptake hypothesis by examining the
363 magnitude of $\gamma(\text{ClNO}_2)$ needed to explain the nocturnal increase in Cl_2 mixing ratios and the
364 dependence of $\gamma(\text{ClNO}_2)$ on its known influencing factors. Assuming a unity yield of Cl_2 from
365 ClNO_2 uptake, the increasing rate of Cl_2 mixing ratios was calculated with Eq. (12). Eq. (13),



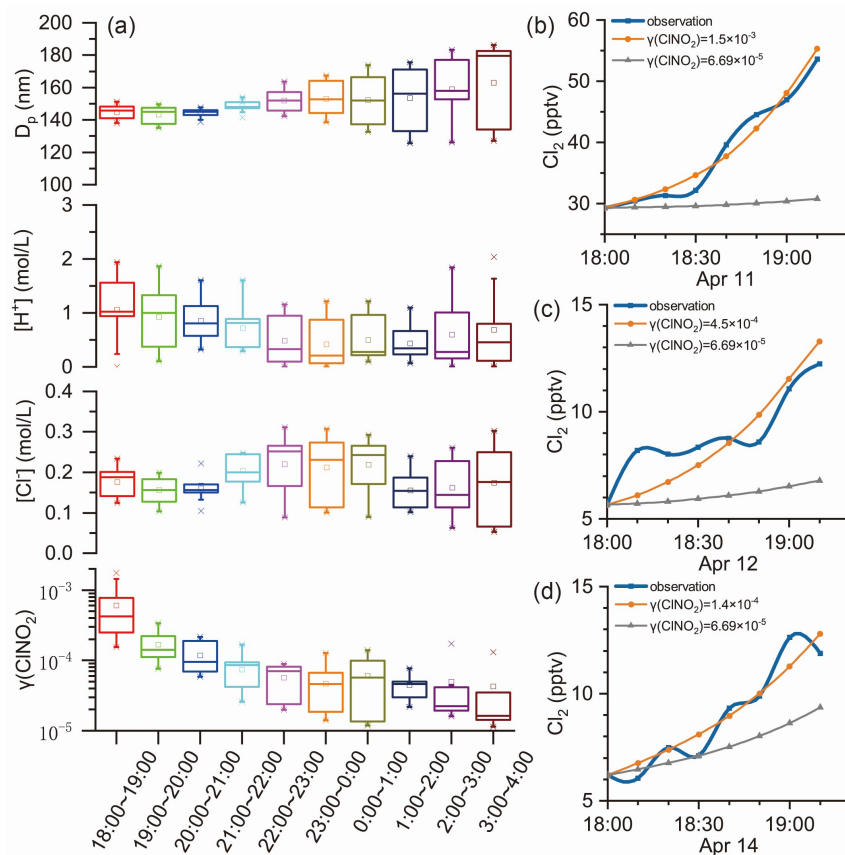
366 which was derived by rearrangement of Eq. (12), was adopted to estimate $\gamma(\text{ClNO}_2)$ via the
367 observed Cl_2 and ClNO_2 levels.

$$368 \quad d[\text{Cl}_2]/dt = \frac{1}{4}c(\text{ClNO}_2)S_a\gamma(\text{ClNO}_2)[\text{ClNO}_2] \quad (12)$$

$$369 \quad \gamma(\text{ClNO}_2)_{\text{obs}} = \frac{4d[\text{Cl}_2]/dt}{c(\text{ClNO}_2)S_a[\text{ClNO}_2]} \quad (13)$$

370 where $c(\text{ClNO}_2)$ is the mean molecular velocity of ClNO_2 (m/s), and $[\text{ClNO}_2]$ represents the
371 averaged ambient concentration of ClNO_2 in the cases of interest.

372 $\gamma(\text{ClNO}_2)_{\text{obs}}$ was estimated in the selected cases following criteria 1 and 2 in Section 3.3, and
373 a steady increase in Cl_2 mixing ratios was required. The resulting values of $\gamma(\text{ClNO}_2)_{\text{obs}}$ were
374 compiled according to the local time and are presented in box charts (Fig. 6a). Fig. 6a also
375 shows the potential factors influencing $\gamma(\text{ClNO}_2)$: $[\text{Cl}^-]$, $[\text{H}^+]$, and particle diameters (D_p ,
376 derived from the ratio of wet V_a to S_a). Here, $[\text{Cl}^-]$ and D_p were regarded as the factors
377 influencing $\gamma(\text{ClNO}_2)$ because a previous field study had found positive correlations of $\gamma(\text{ClNO}_2)$
378 with $[\text{Cl}^-]$ and D_p (Haskins et al., 2019). $[\text{H}^+]$ was considered because the previous laboratory
379 study proposed that H^+ was as a reactant in Cl_2 production (Roberts et al., 2008). Each box
380 represents the $\gamma(\text{ClNO}_2)$, $[\text{Cl}^-]$, $[\text{H}^+]$, or D_p of 10-min resolutions derived on individual days.
381 For example, the box for 18:00–19:00 contains the $\gamma(\text{ClNO}_2)$ estimated at 18:00–19:00 on 11,
382 12, and 14 April (Fig. 6b–6d). Fig. 6b–6d displays the observed Cl_2 levels and the projected
383 trend of Cl_2 levels obtained by use of Eq. (12).



384

385 **Figure 6.** $\gamma(CINO_2)$ estimated using field observation data. (a) $\gamma(CINO_2)_{obs}$, $[Cl^-]$, $[H^+]$, and D_p
 386 estimated at various nighttime periods. (b)–(d) Trends of increasing trends of Cl_2 mixing ratios
 387 during the early evening hours on 11, 12, and 14 April, respectively. Orange and gray lines
 388 represent the projected trend of Cl_2 mixing ratios using Eq. (12) with constant $\gamma(CINO_2)$ values
 389 and observed $CINO_2$ levels.

390

391 As the increasing rate of Cl_2 concentrations ($d[Cl_2]/dt$) did not change significantly during
 392 the night (Fig. 5d), the $\gamma(CINO_2)$ value was constrained by a sharp decreasing trend to
 393 compensate for the increasing $CINO_2$ levels after dusk (see Eq. 12). The highest $\gamma(CINO_2)_{obs}$
 394 value determined during the early evening hours (18:00–19:00) was similar to the laboratory-
 395 derived $\gamma(CINO_2)$ value on acidic salt films (6×10^{-3}) (Roberts et al., 2008). However, the lowest
 396 $\gamma(CINO_2)_{obs}$ value estimated during later nighttime hours (22:00–04:00) was two orders of



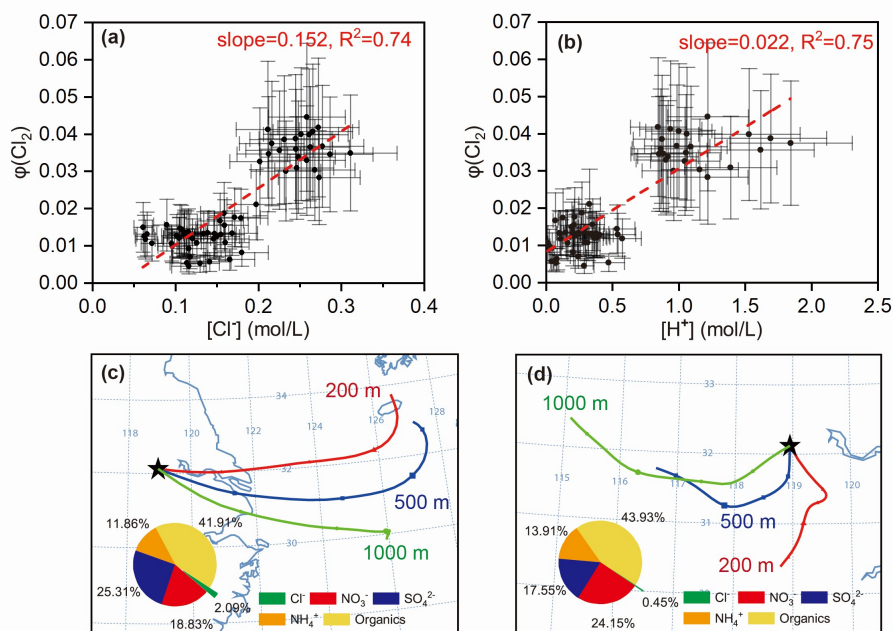
397 magnitude lower (10^{-5}) and was comparable that observed during previous field observations
398 (Haskins et al., 2019). The large variations in the $\gamma(\text{ClNO}_2)$ value contrasted with the relatively
399 stable levels of $[\text{Cl}^-]$, $[\text{H}^+]$, and D_p at various times of night, which is in opposition to the current
400 understanding of the relationship between the $\gamma(\text{ClNO}_2)$ and these factors. Therefore, the ClNO_2
401 uptake hypothesis cannot explain the nocturnal increase in Cl_2 mixing ratios that we observed
402 at our study site. We propose another hypothesis for the ClNO_2 – Cl_2 correlation and suggest that
403 Cl_2 is a co-product of ClNO_2 produced from N_2O_5 uptake, in which ClNO_2 is not necessarily an
404 intermediate of Cl_2 . However, further studies are needed to validate this hypothesis.

405 3.4.2 Parameterizing Cl_2 formation from N_2O_5 uptake

406 As the nighttime Cl_2 , ClNO_2 , and most nitrate ultimately originated from N_2O_5 uptake, we
407 can derive a relationship between Cl_2 and the N_2O_5 uptake. We assigned a production yield to
408 Cl_2 ($\varphi(\text{Cl}_2)$) from the N_2O_5 uptake analogous to the ClNO_2 yield and calculated this using Eq.
409 (14):

$$410 \quad \varphi(\text{Cl}_2) = \frac{d[\text{Cl}_2]/dt}{k(\text{N}_2\text{O}_5)[\text{N}_2\text{O}_5]} \quad (14)$$

411 $\varphi(\text{Cl}_2)$ was estimated in the same cases in which $\gamma(\text{N}_2\text{O}_5)$ and $\varphi(\text{ClNO}_2)$ were derived, because
412 the availability of $\gamma(\text{N}_2\text{O}_5)$ was a prerequisite of deriving $\varphi(\text{Cl}_2)$. The estimated $\varphi(\text{Cl}_2)$ value
413 was 0.01–0.04 (Table S2). The dependences of $\varphi(\text{Cl}_2)$ on its potential influencing factors (i.e.,
414 $[\text{Cl}^-]$, $[\text{H}^+]$, and D_p) were examined. The results show that $\varphi(\text{Cl}_2)$ had positive correlations with
415 both $[\text{Cl}^-]$ ($R^2 = 0.74$) and $[\text{H}^+]$ ($R^2 = 0.75$) and that the data had a high $\varphi(\text{Cl}_2)$ region and a low
416 $\varphi(\text{Cl}_2)$ region (Fig. 7a, b). The low $\varphi(\text{Cl}_2)$ values were found in continental air masses with
417 relatively lower chloride concentrations, more alkaline ammonium, less acidic sulfate and
418 nitrate, and thus lower acidity (Fig. 7d), whereas the high $\varphi(\text{Cl}_2)$ values were associated with
419 marine air masses with higher loadings of aerosol chloride, less ammonium, and more acidic
420 compounds, and thus higher acidity (Fig. 7c). The higher acidity in the marine air masses may
421 be explained by the passage of this air mass over the industrialized cities in the YRD where
422 large concentrations of SO_2 and NO_x are emitted. The dependences of the defined $\varphi(\text{Cl}_2)$ on
423 $[\text{Cl}^-]$ and $[\text{H}^+]$ indicate that nocturnal Cl_2 production requires the presence of highly acidic
424 chloride-rich particles and sufficient levels of N_2O_5 .



425
 426 **Figure 7.** Estimated $\phi(\text{Cl}_2)$ from N_2O_5 uptake and the factors influencing $\phi(\text{Cl}_2)$ (a) and (b)
 427 Dependencies of $\phi(\text{Cl}_2)$ on $[\text{Cl}^-]$ and $[\text{H}^+]$ in selected cases. (c) and (d) are examples of high
 428 $\phi(\text{Cl}_2)$ values in marine air masses (e.g., 13 April) and low $\phi(\text{Cl}_2)$ values in inland air masses
 429 (e.g., 18 April) represented by 24-hour backward trajectories. Inserted pie charts show average
 430 aerosol chemical compositions during 21:40 on 12 April to 00:40 on 13 April and from 22:20
 431 to 23:40 17 April, respectively.

432
 433 A parameterization scheme is derived based on the dependences of $\phi(\text{Cl}_2)$ on $[\text{Cl}^-]$ and $[\text{H}^+]$
 434 to predict the Cl_2 formation involving N_2O_5 heterogeneous chemistry. Mechanistically, it is
 435 assumed that the nocturnal Cl_2 is produced from reactions involving NO_2^+ . The production rates
 436 of nitrate, ClNO_2 , and Cl_2 from the loss of NO_2^+ are expressed in Eq. (15) through Eq. (17). The
 437 loss rate of aerosol organics induced by NO_2^+ is expressed in Eq. (18) (noted as $d[\text{Org}]/dt$ here).
 438
$$d[\text{NO}_3^-]/dt = k_3[\text{NO}_2^+][\text{H}_2\text{O}] \quad (15)$$

 439
$$d[\text{ClNO}_2]/dt = k_4[\text{NO}_2^+][\text{Cl}^-] \quad (16)$$

 440
$$d[\text{Cl}_2]/dt = k_6[\text{NO}_2^+][\text{Cl}^-][\text{H}^+] \quad (17)$$

 441
$$d[\text{Org}]/dt = k_5[\text{NO}_2^+][\text{Org}] \quad (18)$$



442 The symbol k_6 represents the rate constant of the reaction involving NO_2^+ , Cl^- , and H^+ . $\varphi(\text{Cl}_2)$
443 is obtained as follows, by assuming a steady state of the NO_2^+ intermediate (Bertram and
444 Thornton, 2009) (Eq. (19)).

$$445 \quad \varphi(\text{Cl}_2) = \frac{\frac{d[\text{Cl}_2]}{dt}}{\frac{d[\text{Cl}_2]}{dt} + \frac{d[\text{ClNO}_2]}{dt} + \frac{d[\text{NO}_3]}{dt} + \frac{d[\text{Org}]}{dt}} = \frac{k_6[\text{Cl}^-][\text{H}^+]}{k_6[\text{Cl}^-][\text{H}^+] + k_4[\text{Cl}^-] + k_3[\text{H}_2\text{O}] + k_5[\text{Org}]} \quad (19)$$

446 To remain consistent with the $\varphi(\text{ClNO}_2)$ parameterizations, the values 483 and 2.05 were
447 adopted for k_4/k_3 and k_5/k_3 , respectively, while k_6/k_3 was estimated from the fitting of $\varphi(\text{Cl}_2)$
448 using Eq. (19) to achieve the least-squares errors between the observed and parameterized $\varphi(\text{Cl}_2)$
449 values. The parameterization of $\varphi(\text{Cl}_2)$ was then expressed as follows (Eq. (20)):

$$450 \quad \varphi(\text{Cl}_2) = \frac{19.38[\text{H}^+][\text{Cl}^-]}{19.38[\text{H}^+][\text{Cl}^-] + 483[\text{Cl}^-] + [\text{H}_2\text{O}] + 2.05[\text{Org}]} \quad (20)$$

451 where the units of $[\text{H}^+]$, $[\text{Cl}^-]$, and $[\text{Org}]$ are mol/L.

452 The previous ClNO_2 uptake method assumed a unity Cl_2 yield from ClNO_2 uptake, but no
453 such assumption is required in the new method for an explicit definition (Eq. 14) and
454 parameterization (Eq. 20) of the $\varphi(\text{Cl}_2)$. In addition, a quantitative relationship between $\varphi(\text{Cl}_2)$
455 and aerosol acidity is established, which was not given in the previous parameterization.

456

457 4. Summary and conclusions

458 This study reports the presence of significant levels of ClNO_2 and Cl_2 at a suburban site in
459 east China. A rapid increase in the ClNO_2 mixing ratios was found to occur after midnight due
460 to larger rates of N_2O_5 heterogeneous loss than in early nighttime hours, and a high $\varphi(\text{ClNO}_2)$
461 value was also responsible for the elevated ClNO_2 mixing ratios. Improved parameterization of
462 $\varphi(\text{ClNO}_2)$ was achieved by involving the suppression effect of aerosol organics. We suggest
463 that the observed nighttime Cl_2 was co-produced with ClNO_2 from the heterogeneous N_2O_5
464 uptake on acidic aerosols that bear high concentrations of chloride, and we also propose a
465 parameterization for $\varphi(\text{Cl}_2)$. The combination of $\varphi(\text{Cl}_2)$, $\varphi(\text{ClNO}_2)$, and $\gamma(\text{N}_2\text{O}_5)$ can be used to
466 predict the nighttime formation of Cl_2 and ClNO_2 from N_2O_5 uptake and their effect on the next
467 day's atmospheric photochemistry.

468



469 *Acknowledgments.* This study was supported by the National Natural Science Foundation
470 of China (NSFC) project (grant number: 91544213 and D0512/41675145), and the Hong
471 Kong Research Grants Council (T24-504/17-N). The authors acknowledge helpful
472 opinions and discussions from Dr. Yee Jun Tham.

473 *Author contributions.* TW designed the research. WN and AD managed the sampling sites. MX,
474 XP, and WW performed the CIMS measurements. CY, ZX, PS, YL, YL, ZX provided other
475 data. MX and TW wrote the manuscript with comments from all co-authors.

476 *Competing interests.* The authors declare that they have no conflict of interest.

477 *Data availability.* To request the CIMS, jNO₂, and NO_y data described in this study, please
478 contact the corresponding author (cetwang@polyu.edu.hk). Other datasets are available by
479 contacting Dr. Wei Nie (niewei@nju.edu.cn).

480

481 **References**

- 482 Ammann, M., Cox, R. A., Crowley, J. N., Jenkin, M. E., Mellouki, A., Rossi, M. J., Troe, J.,
483 and Wallington, T. J.: Evaluated kinetic and photochemical data for atmospheric chemistry:
484 Volume VI – heterogeneous reactions with liquid substrates, *Atmos. Chem. Phys.*, 13, 8045-
485 8228, 10.5194/acp-13-8045-2013, 2013.
- 486 Behnke, W., George, C., Scheer, V., and Zetzsch, C.: Production and decay of ClNO₂ from the
487 reaction of gaseous N₂O₅ with NaCl solution: Bulk and aerosol experiments, *Journal of*
488 *Geophysical Research: Atmospheres*, 102, 3795-3804, 1997.
- 489 Bertram, T., and Thornton, J.: Toward a general parameterization of N₂O₅ reactivity on aqueous
490 particles: the competing effects of particle liquid water, nitrate and chloride, *Atmospheric*
491 *Chemistry and Physics*, 9, 8351-8363, 2009.
- 492 Custard, K. D., Pratt, K. A., Wang, S., and Shepson, P. B.: Constraints on Arctic Atmospheric
493 Chlorine Production through Measurements and Simulations of Cl₂ and ClO, *Environmental*
494 *Science & Technology*, 50, 12394-12400, 10.1021/acs.est.6b03909, 2016.
- 495 Deiber, G., George, C., Calvé, S. L., Schweitzer, F., and Mirabel, P.: Uptake study of ClONO₂
496 and BrONO₂ by Halide containing droplets, *Atmospheric Chemistry and Physics*, 4, 1291-1299,
497 2004.
- 498 Ding, A., Fu, C., Yang, X., Sun, J., Zheng, L., Xie, Y., Herrmann, E., Nie, W., Petäjä, T., and
499 Kerminen, V.-M.: Ozone and fine particle in the western Yangtze River Delta: an overview of
500 1 yr data at the SORPES station, *Atmospheric Chemistry and Physics*, 13, 5813-5830, 2013.
- 501 Ding, A., Huang, X., Nie, W., Chi, X., Xu, Z., Zheng, L., Xu, Z., Xie, Y., Qi, X., and Shen, Y.:
502 Significant reduction of PM_{2.5} in eastern China due to regional-scale emission control: evidence
503 from SORPES in 2011–2018, *Atmospheric Chemistry and Physics*, 19, 11791-11801, 2019.
- 504 Finlayson-Pitts, B., Ezell, M., and Pitts, J.: Formation of chemically active chlorine compounds



- 505 by reactions of atmospheric NaCl particles with gaseous N_2O_5 and ClONO_2 , *Nature*, 337, 241-
506 244, 1989.
- 507 Haskins, J. D., Lee, B. H., Lopez-Hilfiker, F. D., Peng, Q., Jaeglé, L., Reeves, J. M., Schroder,
508 J. C., Campuzano-Jost, P., Fibiger, D., and McDuffie, E. E.: Observational constraints on the
509 formation of Cl_2 from the reactive uptake of ClONO_2 on aerosols in the polluted marine boundary
510 layer, *Journal of Geophysical Research: Atmospheres*, 124, 8851-8869, 2019.
- 511 Kercher, J., Riedel, T., and Thornton, J.: Chlorine activation by N_2O_5 : simultaneous, in situ
512 detection of ClONO_2 and N_2O_5 by chemical ionization mass spectrometry, *Atmospheric*
513 *Measurement Techniques*, 2, 193-204, 2009.
- 514 Lewis, E. R.: An examination of Köhler theory resulting in an accurate expression for the
515 equilibrium radius ratio of a hygroscopic aerosol particle valid up to and including relative
516 humidity 100%, *Journal of Geophysical Research: Atmospheres*, 113, 2008.
- 517 Liao, J., Huey, L. G., Liu, Z., Tanner, D. J., Cantrell, C. A., Orlando, J. J., Flocke, F. M., Shepson,
518 P. B., Weinheimer, A. J., and Hall, S. R.: High levels of molecular chlorine in the Arctic
519 atmosphere, *Nature Geoscience*, 7, 91, 2014.
- 520 Liu, X., Qu, H., Huey, L. G., Wang, Y., Sjostedt, S., Zeng, L., Lu, K., Wu, Y., Hu, M., and Shao,
521 M.: High levels of daytime molecular chlorine and nitryl chloride at a rural site on the North
522 China Plain, *Environmental science & technology*, 51, 9588-9595, 2017.
- 523 McDuffie, E. E., Fibiger, D. L., Dubé, W. P., Lopez-Hilfiker, F., Lee, B. H., Thornton, J. A.,
524 Shah, V., Jaeglé, L., Guo, H., and Weber, R. J.: Heterogeneous N_2O_5 uptake during winter:
525 Aircraft measurements during the 2015 WINTER campaign and critical evaluation of current
526 parameterizations, *Journal of Geophysical Research: Atmospheres*, 123, 4345-4372, 2018a.
- 527 McDuffie, E. E., Fibiger, D. L., Dubé, W. P., Lopez-Hilfiker, F., Lee, B. H., Jaeglé, L., Guo, H.,
528 Weber, R. J., Reeves, J. M., and Weinheimer, A. J.: ClONO_2 yields from aircraft measurements
529 during the 2015 WINTER campaign and critical evaluation of the current parameterization,
530 *Journal of Geophysical Research: Atmospheres*, 123, 9094-9130, 2018b.
- 531 McNamara, S. M., Raso, A. R., Wang, S., Thanekar, S., Boone, E. J., Kolesar, K. R., Peterson,
532 P. K., Simpson, W. R., Fuentes, J. D., and Shepson, P. B.: Springtime Nitrogen Oxide-
533 Influenced Chlorine Chemistry in the Coastal Arctic, *Environmental science & technology*,
534 2019.
- 535 Mielke, L. H., Furgeson, A., and Osthoff, H. D.: Observation of ClONO_2 in a mid-continental
536 urban environment, *Environ Sci Technol*, 45, 8889-8896, 10.1021/es201955u, 2011.
- 537 Molina, M. J., and Rowland, F. S.: Stratospheric sink for chlorofluoromethanes: chlorine atom-
538 catalysed destruction of ozone, *Nature*, 249, 810, 1974.
- 539 Morgan, W., Ouyang, B., Allan, J., Aruffo, E., Di Carlo, P., Kennedy, O., Lowe, D., Flynn, M.,
540 Rosenberg, P., and Williams, P.: Influence of aerosol chemical composition on N_2O_5 uptake:
541 airborne regional measurements in northwestern Europe, *Atmospheric Chemistry and Physics*,
542 15, 973-990, 2015.
- 543 Osthoff, H. D., Roberts, J. M., Ravishankara, A. R., Williams, E. J., Lerner, B. M., Sommariva,
544 R., Bates, T. S., Coffman, D., Quinn, P. K., Dibb, J. E., Stark, H., Burkholder, J. B., Talukdar,
545 R. K., Meagher, J., Fehsenfeld, F. C., and Brown, S. S.: High levels of nitryl chloride in the
546 polluted subtropical marine boundary layer, *Nature Geoscience*, 1, 324-328, 10.1038/ngeo177,



- 547 2008.
- 548 Phillips, G. J., Thieser, J., Tang, M., Sobanski, N., Schuster, G., Fachinger, J., Drewnick, F.,
549 Borrmann, S., Bingemer, H., and Lelieveld, J.: Estimating N_2O_5 uptake coefficients using
550 ambient measurements of NO_3 , N_2O_5 , ClNO_2 and particle-phase nitrate, *Atmospheric*
551 *Chemistry and Physics*, 16, 13231-13249, 2016.
- 552 Pratte, P., and Rossi, M. J.: The heterogeneous kinetics of HOBr and HOCl on acidified sea salt
553 and model aerosol at 40–90% relative humidity and ambient temperature, *Physical Chemistry*
554 *Chemical Physics*, 8, 3988-4001, 2006.
- 555 Priestley, M., Breton, M. I., Bannan, T. J., Worrall, S. D., Bacak, A., Smedley, A. R., Reyes-
556 Villegas, E., Mehra, A., Allan, J., and Webb, A. R.: Observations of organic and inorganic
557 chlorinated compounds and their contribution to chlorine radical concentrations in an urban
558 environment in northern Europe during the wintertime, *Atmospheric Chemistry and Physics*,
559 18, 13481-13493, 2018.
- 560 Qiu, X., Ying, Q., Wang, S., Duan, L., Zhao, J., Xing, J., Ding, D., Sun, Y., Liu, B., and Shi, A.:
561 Modeling the impact of heterogeneous reactions of chlorine on summertime nitrate formation
562 in Beijing, China, *Atmospheric Chemistry and Physics*, 19, 6737-6747, 2019.
- 563 Riedel, T. P., Bertram, T. H., Crisp, T. A., Williams, E. J., Lerner, B. M., Vlasenko, A., Li, S.
564 M., Gilman, J., de Gouw, J., Bon, D. M., Wagner, N. L., Brown, S. S., and Thornton, J. A.:
565 Nitryl chloride and molecular chlorine in the coastal marine boundary layer, *Environ Sci*
566 *Technol*, 46, 10463-10470, 10.1021/es204632r, 2012.
- 567 Riedel, T. P., Wagner, N. L., Dubé, W. P., Middlebrook, A. M., Young, C. J., Öztürk, F., Bahreini,
568 R., VandenBoer, T. C., Wolfe, D. E., and Williams, E. J.: Chlorine activation within urban or
569 power plant plumes: Vertically resolved ClNO_2 and Cl_2 measurements from a tall tower in a
570 polluted continental setting, *Journal of Geophysical Research: Atmospheres*, 118, 8702-8715,
571 2013.
- 572 Roberts, J. M., Osthoff, H. D., Brown, S. S., and Ravishankara, A.: N_2O_5 oxidizes chloride to
573 Cl_2 in acidic atmospheric aerosol, *Science*, 321, 1059-1059, 2008.
- 574 Roberts, J. M., Osthoff, H. D., Brown, S. S., Ravishankara, A., Coffman, D., Quinn, P., and
575 Bates, T.: Laboratory studies of products of N_2O_5 uptake on Cl^- containing substrates,
576 *Geophysical Research Letters*, 36, 2009.
- 577 Seinfeld, J. H., and Pandis, S. N.: *Atmospheric chemistry and physics: from air pollution to*
578 *climate change*, John Wiley & Sons, 2016.
- 579 Simpson, W. R., Brown, S. S., Saiz-Lopez, A., Thornton, J. A., and von Glasow, R.:
580 Tropospheric halogen chemistry: Sources, cycling, and impacts, *Chemical reviews*, 115, 4035-
581 4062, 2015.
- 582 Spicer, C., Chapman, E., Finlayson-Pitts, B., Plastringe, R., Hubbe, J., Fast, J., and Berkowitz,
583 C.: Unexpectedly high concentrations of molecular chlorine in coastal air, *Nature*, 394, 353,
584 1998.
- 585 Staudt, S., Gord, J. R., Karimova, N., McDuffie, E. E., Brown, S. S., Gerber, R. B., Nathanson,
586 G. M., and Bertram, T. H.: Sulfate and Carboxylate Suppress the Formation of ClNO_2 at
587 Atmospheric Interfaces, *ACS Earth and Space Chemistry*, 2019.
- 588 Sun, P., Nie, W., Chi, X., Xie, Y., Huang, X., Xu, Z., Qi, X., Xu, Z., Wang, L., and Wang, T.:



- 589 Two years of online measurement of fine particulate nitrate in the western Yangtze River Delta:
590 influences of thermodynamics and N_2O_5 hydrolysis, *Atmospheric Chemistry and Physics*, 18,
591 17177-17190, 2018.
- 592 Tham, Y. J., Wang, Z., Li, Q., Yun, H., Wang, W., Wang, X., Xue, L., Lu, K., Ma, N., Bohn, B.,
593 Li, X., Kecorius, S., Größ, J., Shao, M., Wiedensohler, A., Zhang, Y., and Wang, T.: Significant
594 concentrations of nitryl chloride sustained in the morning: investigations of the causes and
595 impacts on ozone production in a polluted region of northern China, *Atmospheric Chemistry
596 and Physics*, 16, 14959-14977, 10.5194/acp-16-14959-2016, 2016.
- 597 Tham, Y. J., Wang, Z., Li, Q., Wang, W., Wang, X., Lu, K., Ma, N., Yan, C., Kecorius, S., and
598 Wiedensohler, A.: Heterogeneous N_2O_5 uptake coefficient and production yield of ClNO_2 in
599 polluted northern China: Roles of aerosol water content and chemical composition, 2018.
- 600 Thornton, J. A., Braban, C. F., and Abbatt, J. P.: N_2O_5 hydrolysis on sub-micron organic aerosols:
601 The effect of relative humidity, particle phase, and particle size, *Physical Chemistry Chemical
602 Physics*, 5, 4593-4603, 2003.
- 603 Thornton, J. A., Kercher, J. P., Riedel, T. P., Wagner, N. L., Cozic, J., Holloway, J. S., Dube, W.
604 P., Wolfe, G. M., Quinn, P. K., Middlebrook, A. M., Alexander, B., and Brown, S. S.: A large
605 atomic chlorine source inferred from mid-continental reactive nitrogen chemistry, *Nature*, 464,
606 271-274, 10.1038/nature08905, 2010.
- 607 Wang, T., Tham, Y. J., Xue, L., Li, Q., Zha, Q., Wang, Z., Poon, S. C., Dubé, W. P., Blake, D.
608 R., and Louie, P. K.: Observations of nitryl chloride and modeling its source and effect on ozone
609 in the planetary boundary layer of southern China, *Journal of Geophysical Research:
610 Atmospheres*, 121, 2476-2489, 2016.
- 611 Wang, X., Jacob, D. J., Eastham, S. D., Sulprizio, M. P., Zhu, L., Chen, Q., Alexander, B.,
612 Sherwen, T., Evans, M. J., Lee, B. H., Haskins, J. D., Lopez-Hilfiker, F. D., Thornton, J. A.,
613 Huey, G. L., and Liao, H.: The role of chlorine in global tropospheric chemistry, *Atmos. Chem.
614 Phys.*, 19, 3981-4003, 10.5194/acp-19-3981-2019, 2019.
- 615 Wexler, A. S.: Atmospheric aerosol models for systems including the ions H^+ , NH_4^+ , Na^+ , SO_4^{2-} ,
616 NO_3^- , Cl^- , Br^- , and H_2O , *Journal of Geophysical Research*, 107, 10.1029/2001jd000451, 2002.
- 617 Yun, H., Wang, W., Wang, T., Xia, M., Yu, C., Wang, Z., Poon, S. C., Yue, D., and Zhou, Y.:
618 Nitrate formation from heterogeneous uptake of dinitrogen pentoxide during a severe winter
619 haze in southern China, *Atmospheric Chemistry and Physics*, 18, 17515-17527, 2018.
- 620 Zhou, Y., Zhao, Y., Mao, P., Zhang, Q., Zhang, J., Qiu, L., and Yang, Y.: Development of a high-
621 resolution emission inventory and its evaluation and application through air quality modeling
622 for Jiangsu Province, China, *Atmospheric Chemistry and Physics*, 17, 211-233, 2017.